



A facile one-pot hydrothermal synthesis of cobalt sulfide nanospheres integrated with graphene nanocomposite as electrode material for high-performance supercapacitors

Ranjith Balu^{1,*}  and Arivuoli Dakshanamoorthy¹

¹Crystal Growth Centre, Anna University, Chennai, Tamil Nadu, India

Received: 13 October 2021

Accepted: 27 February 2022

Published online:
14 March 2022

© The Author(s), under exclusive licence to Springer Science+Business Media, LLC, part of Springer Nature 2022

ABSTRACT

Transition metal chalcogenides have fascinating characteristics are considered as electrode materials for high-performance energy storage devices. Herein, we report the CoS/G nanocomposite was successfully synthesized by a simple one-pot hydrothermal method. The phase formation and morphology of the obtained materials were analyzed by various techniques. The electrochemical properties of the prepared electrode materials were assessed from cyclic voltammetry in a three-electrode system. The obtained cyclic voltammetry curves demonstrate pseudocapacitive behavior for prepared materials due to the synergistic effect between Cobalt and sulfur. The Galvanometric Charge Discharge (GCD) profile of the materials confirms the pseudocapacitive nature and specific capacitance calculated from these curves. The CoS/G nanocomposite delivered high specific capacitance 739.83 Fg^{-1} compared to the pure CoS nanospheres 390 Fg^{-1} and prolonged cyclic stability with 91.2% capacity retention after 3000 cycles. Overall, these excellent electrochemical performances indicate the CoS/G nanocomposite as a desirable electrode material for commercial supercapacitor applications.

1 Introduction

In recent times, supercapacitors have gained enormous attention due to their appreciable performance, eco-friendly, easy handling, and energy-efficient applications [1–5]. Supercapacitors deliver high power density and long-term cyclic stability compared to other energy storage devices such as

capacitors [6], fuel cells [7], and batteries [8–10]. The supercapacitors' charge storage mechanism differs from that of batteries in that ions are absorbed and unabsorbed at the electrodes during the charge and discharge process. This mechanism leads to outstanding cyclic stability and high power density. Supercapacitors consist of two conductive electrodes that are separated by an ion-permeable membrane

Address correspondence to E-mail: rbalubio@gmail.com

that is immersed in electrolyte solutions. The electrochemical performance of supercapacitors is determined by the electrode surface area, electrolyte solutions, and voltage range. Supercapacitors are classified into two categories of charge storage mechanisms; the first one is a non-Faradic reaction that occurs at the surface of the electrode, which is called an electric double-layer capacitor [11–13]. Another one is the Faradic process, where oxidation and reduction reactions are involved between the electrode and the electrolyte. Carbonaceous materials, namely carbon black, CNT, and graphene oxide, are used as electrode materials for electric double-layer capacitors [14, 15], whereas, transition metal oxides, metal sulfides, and conducting polymers are used as electrode materials for pseudocapacitors [16–18], which can store more charges than EDLC electrode materials but have low power density and poor cyclic stability. However, the electrochemical performance of both supercapacitors suffered from some parameters. To resolve these issues, carbonaceous materials with transition metal oxide or metal sulfide materials form nanocomposite. This combination improves the performance of the supercapacitor. It's called a hybrid supercapacitor [19, 20]. Because of the synergetic effect between the two materials, these hybrid capacitor combinations have a higher energy density than EDLC and longer cyclic stability than pseudocapacitors. In this manner, carbonaceous materials such as activated carbon, carbon nanotubes, and graphene have been used for energy storage devices due to their high surface area, high conductivity, and prolonged cyclic stability. Among these materials, graphene is the most attractive material in the carbonaceous group due to its desirable properties such as ultra-large surface area ($2600 \text{ m}^2\text{g}^{-1}$), excellent electron mobility, high mechanical strength, and two-dimensional nanostructured materials with a single atom thickness [21, 22]. Furthermore, graphene can prevent the aggregation of nanoparticles in the nanocomposite. The graphene-based composites have been evaluated recently, functionalized on the surface of the graphene, graphene/metal oxide nanocomposite, graphene/conducting polymers, and graphene/metal sulfide composites [23, 24]. These nanocomposites can exhibit both capacitance behaviors, due to the incorporation of the nanoparticles over the surface of the graphene. Recent research has shown that the transition metal sulfides are frequently used for

graphene-based composites for excellent electrochemical performance in hybrid combinations such as Molybdenum sulfide (MoS_2) [25], cadmium sulfide (CdS) [26], Copper sulfide (CuS) [27], Tin sulfide (SnS) [28], Nickel sulfide (NiS) [29], and Zinc sulfide (ZnS) [30], have been reported. Among these various composite materials, $\text{CoS}/\text{graphene}$ is a promising next-generation electrode material because of its intrinsic high electronic conductivity and high specific capacity [31]. In particular, cobalt sulfides (CoS , CoS_2 , and CoS_x) materials are used as composite materials due to their different nanostructures exhibiting excellent electrochemical efficiency [32–34]. For example, high-performance supercapacitor applications, three-dimensional flower-like CoS hierarchitectures, and CoS layers were prepared on graphene nanosheets [35–37]. There is a minimum of the research reported on high-cost synthesis routes and time-consuming methods, and there is a need to study a cost-effective way and a simple approach.

The above idea has been summarized in this work. We report the simple hydrothermal synthesis of spheres like cobalt sulfide decorated graphene nanocomposite. The physicochemical characterizations have been assessed by several techniques to analyze the crystal structures, morphologies, optical and thermal properties. The fabricated CoS/G nanocomposite electrode shows higher performance than pure CoS nanospheres. The nanocomposite electrodes demonstrated maximum specific capacitance and outstanding cyclic stability, 92.68% after 1000 cycles in three-electrode systems. The enhanced performance is due to the intercalation of CoS nanospheres embedded in the graphene sheet. The CoS/G nanocomposite could be a desirable material for supercapacitor applications.

2 Experimental

2.1 Materials and methods

Graphite powder, Cobalt (ii) nitrate dihydrate [$\text{Co}(\text{NO}_3)_2 \cdot 2\text{H}_2\text{O}$], Thiourea (NH_2CSNH_2) and ethanol were obtained from Sigma–Aldrich. Sodium nitrate [NaNO_3], potassium permanganate (KMnO_4), potassium hydroxide [KOH], hydrochloric acid [11.6N], concentrated sulfuric acid [36N] hydrogen peroxide [H_2O_2 , 30%], hydrazine hydrate [$\text{N}_2\text{H}_4 \cdot \text{H}_2\text{O}$, 80%], ethanol, *N*-methyl pyrrolidone (NMP), and

polyvinylidene difluoride (PVDF), were purchased from Merck Chemicals. Deionized water was acquired from the Millipore water purification plant for synthesis and washing purpose.

2.2 Preparation of cobalt sulfide decorated graphene (CoS/G) nanocomposite

In this work, graphene oxide was prepared using the modified Hummers method [38]. In detail, as-prepared graphene oxide (10 mg/mL) was ultrasonically dispersed in deionized water, and then a stoichiometric ratio of 1 mmol of $\text{Co}(\text{NO}_3)_2 \cdot 2\text{H}_2\text{O}$ and 5 mmol of NH_2CSNH_2 was dissolved in the above solution and stirred continuously for another 1 h. The as-prepared mixture was poured into a 100 ml Teflon-lined autoclave, filled up to 80% of its volume, and it was sealed and placed in a muffle furnace at 170 °C for 24 h. Then the autoclave was naturally cooled to ambient temperature, the precipitated particles were taken out, and it was washed several times with water and ethanol. The washed product was dried at 60 °C for 8 h. A similar method was followed by preparing CoS nanospheres without using GO suspension. Scheme 1 depicts a schematic illustration of the preparation of a CoS/G nanocomposite.

2.3 Materials characterization

Powder X-ray diffraction patterns from an X-ray diffractometer (PANalytical X'Pert Powder XRD) employing Cu K radiation (= 1.5406) operating at 40 kV and 40 mA in a 2 θ range of 5°–80° with a scan rate of 8° min⁻¹ were used to assess the phase formation of the prepared materials. The microstructure and morphology of the prepared materials were examined by a scanning electron microscope (Carl Zeiss MA15/EVO 18 Scanning Electron Microscope). The elemental composition and elemental mapping of the obtained samples are investigated by EDA and EDs, along with a scanning electron microscope using (Oxford Instruments Nano Analysis INCA Energy 250 Microanalysis System (EDS)). The thermal stability of the prepared materials was analyzed by TGA analysis by PerkinElmer SII (Diamond series). The Raman spectra of the prepared samples are recorded using room temperature Raman spectroscopy. The functional group and bonding nature of the materials have been recorded by Fourier

transform infrared spectroscopy (FT-IR, PERKIN ELMER RX-1). The UV absorbance of the obtained materials was recorded by the UV-Vis Diffuse Reflectance spectrometer on a (UV-V650, Jasco Instrument, Japan). The specific surface areas of the synthesized materials were characterized by Brinier-Emmett-Teller (BET) measurements (QUADRASORB SI).

2.4 Electrochemical measurements

A classic three-electrode electrochemical system was built to assess the electrochemical performance of the as-synthesized materials. The working electrode was prepared by mixing as-synthesized CoS/G nanocomposite (80 wt%), activated carbon (10 wt%), and polyvinylidene fluoride (10 wt%) into a slurry. The prepared slurry was coated on the surface of the nickel foam (1 cm²). For all of the prepared electrodes, the mass loadings were adjusted to 1.8 mg/cm² and dried at 100 °C for 12 h. The counter and the reference electrode were chosen to be platinum and Ag/AgCl, respectively. The electrochemical studies, such as cyclic voltammetry, Galvanostatic charge/discharge, and electrochemical impedance spectroscopy, were tested in a 3 M KOH aqueous electrolyte solution on a CHI 7001C electrochemical work station. The specific capacitance of the prepared materials was calculated from cyclic voltammograms and Galvanostatic charge discharges according to the following equation.

Specific capacitance from CV

$$C_{\text{sp}} = \int \frac{Idv}{m\Delta V} \quad (1)$$

Specific capacitance from GCD

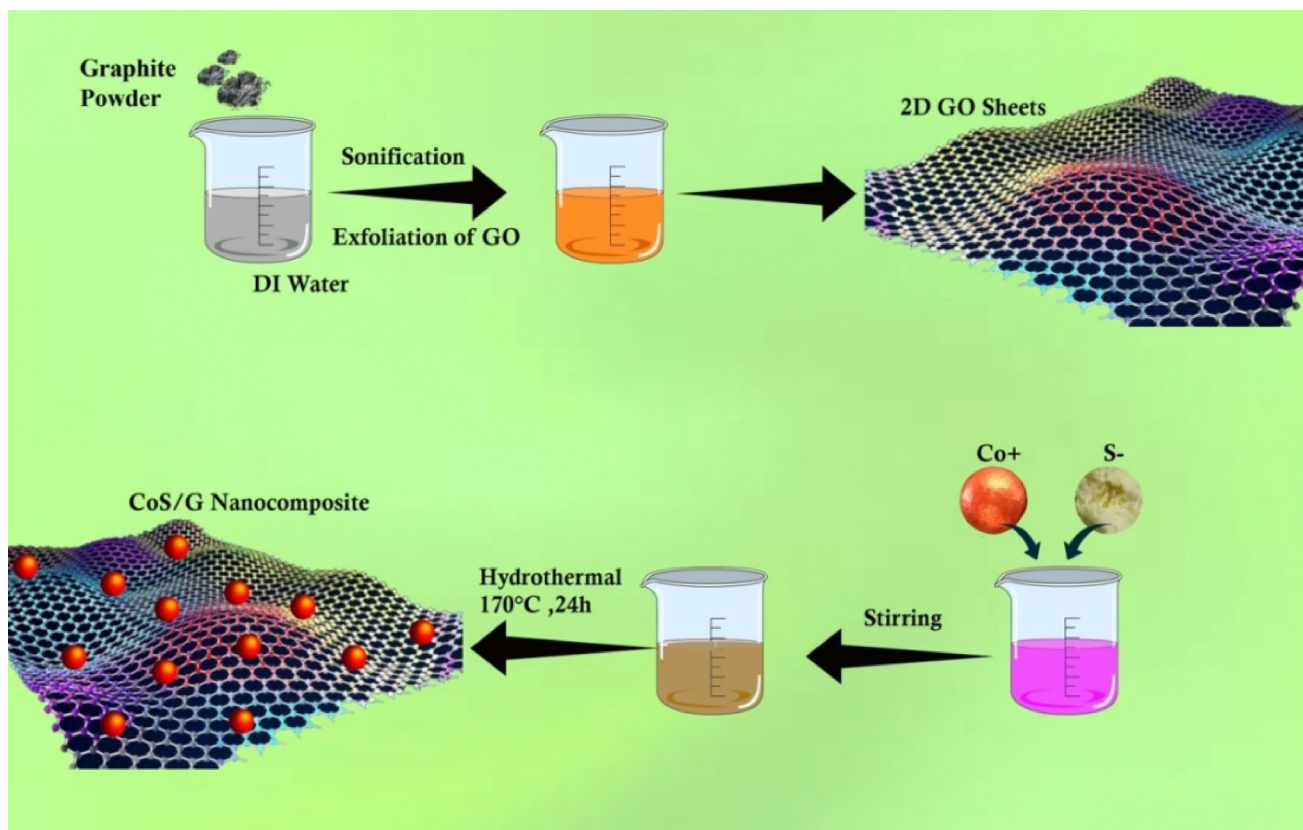
$$C_{\text{sp}} = \frac{I \times \Delta t}{m \times \Delta V} \quad (2)$$

C_{sp} is the specific capacitance (F/g) of the electrode materials, I is the applied current (A), t is the discharge time of one cycle (s), m is the mass of active material (g), and V represents potential window (V).

3 Results and discussion

3.1 Structural studies

The phase identification of the synthesized materials was assessed from powder X-ray diffraction analysis,



Scheme 1 Schematic illustration of the preparation of CoS/G nanocomposite

which is depicted in Fig. 1a. A sharp, intense diffraction peak (001) was observed at 11.2° , which indicates the hexagonal crystal structure of the synthesized graphene oxide [21]. The X-ray diffraction pattern of the CoS nanospheres peaks was observed

at 2θ of 30.6 , 35.3 , 46.9 , and 54.6 , corresponding to (100), (101), (102), and (110) planes of hexagonal CoS (JCPDS card No. 042-0826) [39]. In the case of the CoS/G nanocomposite, the observed diffraction peaks indicate the similar structure of CoS

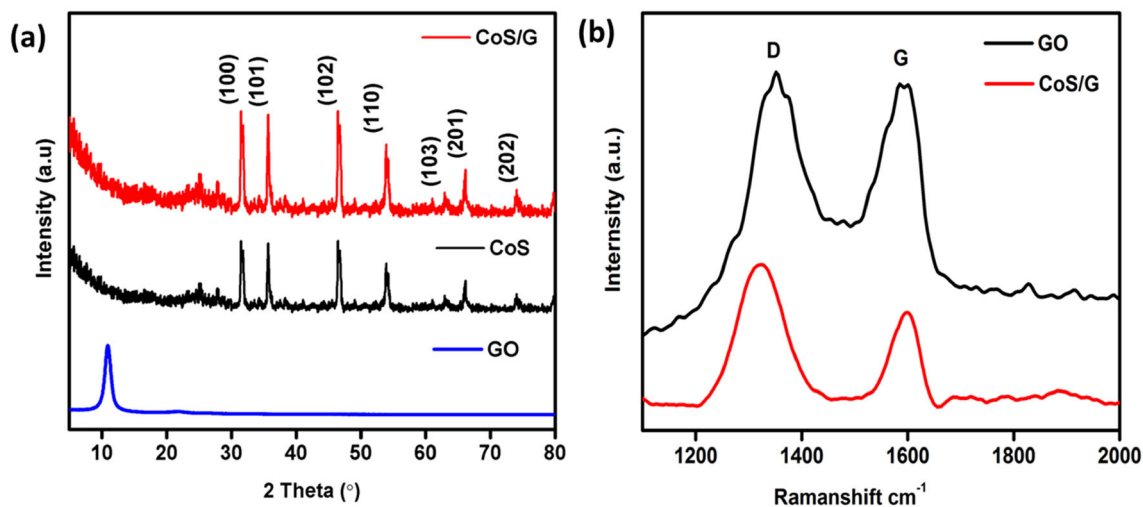


Fig. 1 **a** X-ray diffraction patterns of Graphene oxide, CoS nanospheres, and CoS/G nanocomposite, **b** Raman spectrum of Graphene oxide and CoS/G nanocomposite

nanospheres. Moreover, it should be noted that no standard patterns of graphene (002) have been found in the CoS/G nanocomposite due to the lower amount of graphene or low-intensity diffraction peak. The CoS nanoparticles are dispersed over the graphene sheets, the interconnected architecture of the composite matrix prevents their aggregation. The average crystalline size of the prepared samples was obtained using the Scherrer formula.

$$D = \frac{0.9\lambda}{\beta \cos\theta}. \quad (3)$$

The average crystallite sizes of the CoS and CoS/G composite found to be 64.9 nm and 60.78 nm, respectively.

The structural and electronic properties of the prepared materials were investigated by Raman analysis. The Raman spectra of graphene oxide and the CoS/G composite are illustrated in Fig. 1b. The graphene oxide two peaks appeared at 1327 cm^{-1} and 1574 cm^{-1} , which correspond to the D and G bands. The observed peaks could be ascribed to the structural defects A1g zone-edge and E2g mode and first-order scattering of the E2g mode of graphite carbon. This confirms the formation of graphene oxide [40]. Peaks were observed in the CoS/G nanocomposite D and G, but their intensity was reduced when compared to pure graphene oxide, indicating the reduction of graphene oxide to graphene and confirming the formation of the nanocomposite. In the meantime, the lower intensity of the composite peaks due to the structural changes in graphene sheets might be influenced by structural defects, strain, layer parameters, and various parameters [41]. The intensity ratios of the D band to G band (I_D/I_G) of graphene oxide and CoS/G nanocomposite were calculated. The intensity ratios of graphene oxide and composite were found to be 0.93 and 1.04, respectively. The CoS/G composite materials demonstrate higher than pure graphene oxide wherein the decoration of the CoS nanospheres over the surface of the graphene layer results in the reduction of sp² carbon domains [37, 42, 43]. This evidences the declined restacking degree of graphene sheets after the presence of CoS nanospheres, which is quite consistent with the X-ray diffraction findings.

3.2 UV–Vis. absorption spectrum analysis

To further explore the optical properties of the parent CoS nanospheres and CoS/G nanocomposite, UV spectroscopy analysis was carried out and is given in Fig. 2a. UV spectra depict the optical absorption of CoS nanoparticles and CoS/G nanocomposite in the visible region. The observation of two major bands in the optical absorption spectrum at lower wavelengths, 270 nm and 350 nm, is ascribed to the $n \rightarrow \pi^*$ transition of the graphene and the CoS transition [44]. The Tauc plot was used to determine the energy band of the composite material.

$$(\alpha hv)^n = A(hv - E_g). \quad (4)$$

The bandgap (E_g) value of the CuS/G nanocomposite was measured at 3.2 eV, which demonstrates itself to be a desirable material for high-performance energy storage applications.

3.3 Functional group and thermal analysis

FTIR spectrums are USED to analyze the functional groups of the prepared materials. The functional groups of the graphene oxide and CoS/G nanocomposite are depicted in Fig. 3. The graphene oxide functional groups were located at 1051 cm^{-1} , 1394 cm^{-1} , 1614 cm^{-1} , 1720 cm^{-1} , and 3440 cm^{-1} corresponding to epoxy C–O vibration, C–OH stretching vibration, C = O stretching vibration, and O–H stretching vibration groups, confirming the formation of graphene oxide [21, 45]. In the case of the CoS/G nanocomposite, both CoS nanospheres and graphene functional groups peaks were observed at 526 and 638 cm^{-1} is correlated to the vibrations of N–C–N and C=S in sulfur source, whereas 453 , 859 , and 958 cm^{-1} correspond to N–C=S which confirms the presence of CoS nanospheres in the composite materials [31, 46]. On the other hand, graphene oxide peaks were observed. Interestingly, 3440 cm^{-1} corresponding to O–H stretching vibration intensity has been suppressed due to the reduction of graphene oxide to graphene [47].

The thermal stability of the as-prepared materials was carried out by thermogravimetric analysis which is demonstrated in Fig. 3b. The obtained samples show various thermal behaviors according to their functional groups. The as-prepared graphene oxide decomposed at three different temperature regions, which is the elimination of water and moisture at less

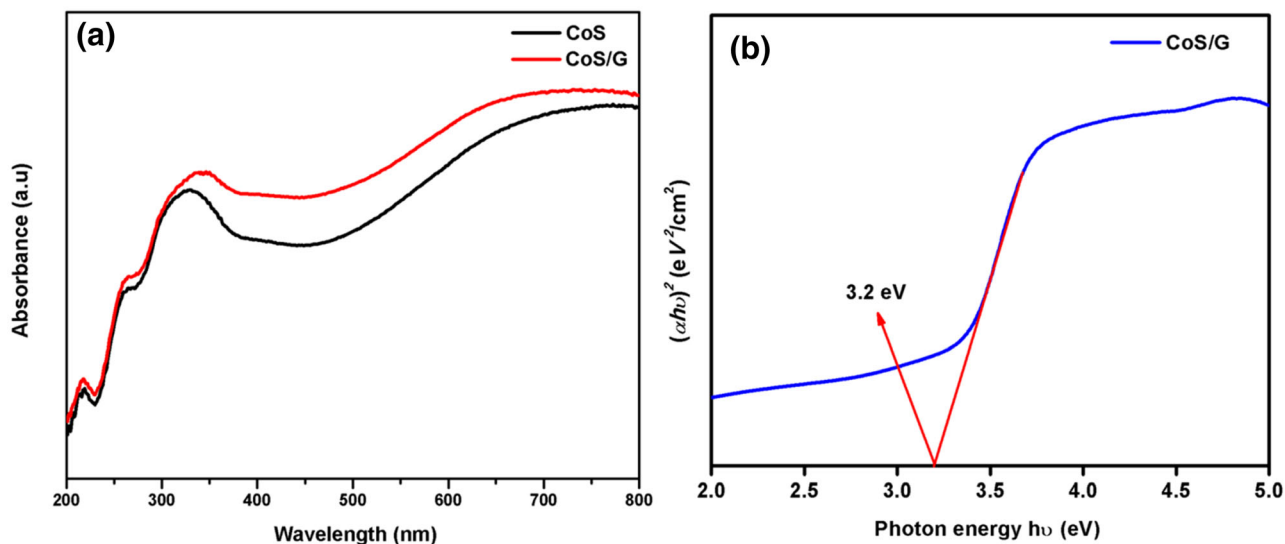


Fig. 2 DRS UV-Vis spectrum of **a** pure CoS nanospheres and CoS/G composite, **b** Optical bandgap of CoS/G nanocomposite

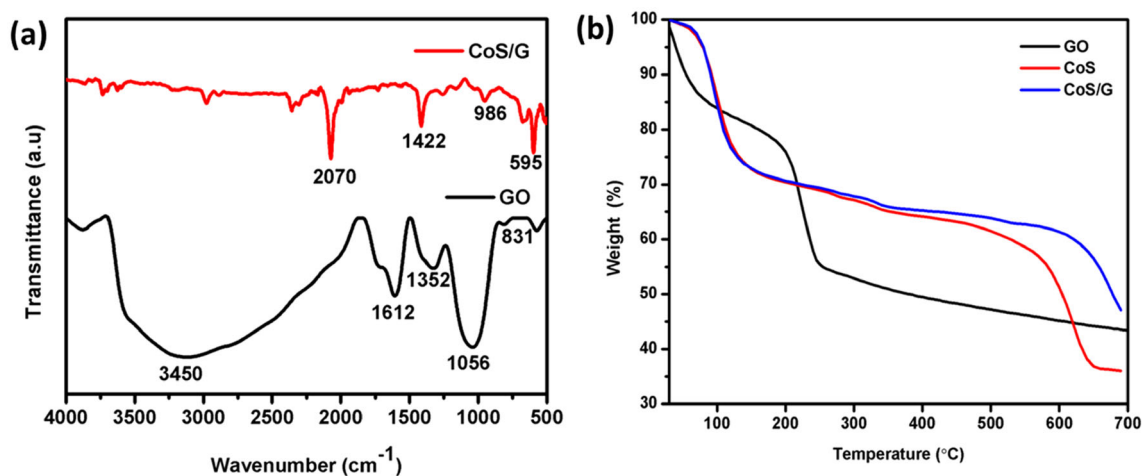


Fig. 3 **a** FTIR spectrum of Graphene oxide and CoS/G nanocomposite. **b** TGA spectrum of Graphene oxide, CoS nanoparticles, and CoS/G nanocomposite

than 100 °C. The major weight loss was observed between 150 and 250 °C due to the decomposition of the graphene oxide into CO, CO₂ and then the gradual weight loss beyond 300 °C which demonstrates the reduction of oxygen functional groups in the graphene oxide [48]. CoS nanospheres show major weight loss from ambient conditions to 100 °C due to the removal of adsorbed water and other contamination. Then the gradual weight loss between 100 and 500 °C might be ascribed to the phase transformation of cobalt sulfides to cobalt oxides owing to exothermal reactions [49]. In the case of

CoS/G nanocomposite, the weight loss features similar to CoS nanospheres were observed but with improved thermal stability as indicated by the increased decomposition temperature. A significant weight loss occurs at 500 °C, supporting the burning of graphene sheets. The graphene oxide and the CoS weight in the CoS/G composite are calculated to be 6% and 94%, respectively. The presence of graphene enhances the thermal stability of the CoS/G nanocomposite, which enhances the cyclic stability during the electrochemical reaction.

3.4 Surface morphology and elemental analysis

The microstructure and morphology of the prepared materials were examined using a scanning electron microscope and a transmission electron microscope, as shown in Figs. 4 and 5. Figure 4a shows the crumpled layer structure of the graphene oxide. Owing to the oxygen functional group, it has a wrinkled and rough texture [40]. The as-obtained CoS had a spherical-like morphology with a wide size distribution, as shown in Fig. 4c. The crumpled layer structure of the graphene sheets was decorated by CoS nanoparticles upon CoS/G nanocomposite formation, which is presented in Fig. 4e, f, h. However, the spherical CoS nanoparticles uniformly embedded in the flake have a heterogeneous size distribution ranging from 30 to 100 nm. The aggregation of the CoS nanospheres was reduced appreciably upon the introduction of the graphene oxide substrate. The morphology of the CoS in the CoS/G nanocomposite differs from the pure spherical CoS nanoparticles. This nanocomposite enhances the specific surface area compared to pure CoS nanoparticles, which will

improve the electrochemical performance. The chemical composition and stoichiometric ratio of the obtained materials were investigated through EDAX analysis along with scanning electron microscopy. The formation of graphene oxide is indicated by the presence of carbon and oxygen peaks as shown in Fig. 4b. The presence of graphene oxide is unambiguously confirmed by the EDAX analysis along with the XRD results. The presence of cobalt and sulfur indicates the formation of pure CoS nanospheres that are depicted in Fig. 4d. In the case of the CoS/G nanocomposite, all the elemental constituents correspond to both the CoS nanospheres and graphene, as seen in Fig. 4f. Furthermore, the elemental mapping of the CoS/G nanocomposite was investigated by EDS elemental mapping in the selected area, which is depicted in Fig. 4i–l. The CoS/G nanocomposite corresponding elements such as C, Co, and S are observed. The element C is distributed homogeneously, and the Co and S distributions are focused primarily on the spherical components, suggesting the existence of CoS nanospheres. In addition, the uniform distribution of the elements Co and S confirms the uniform distribution of CoS nanoparticles

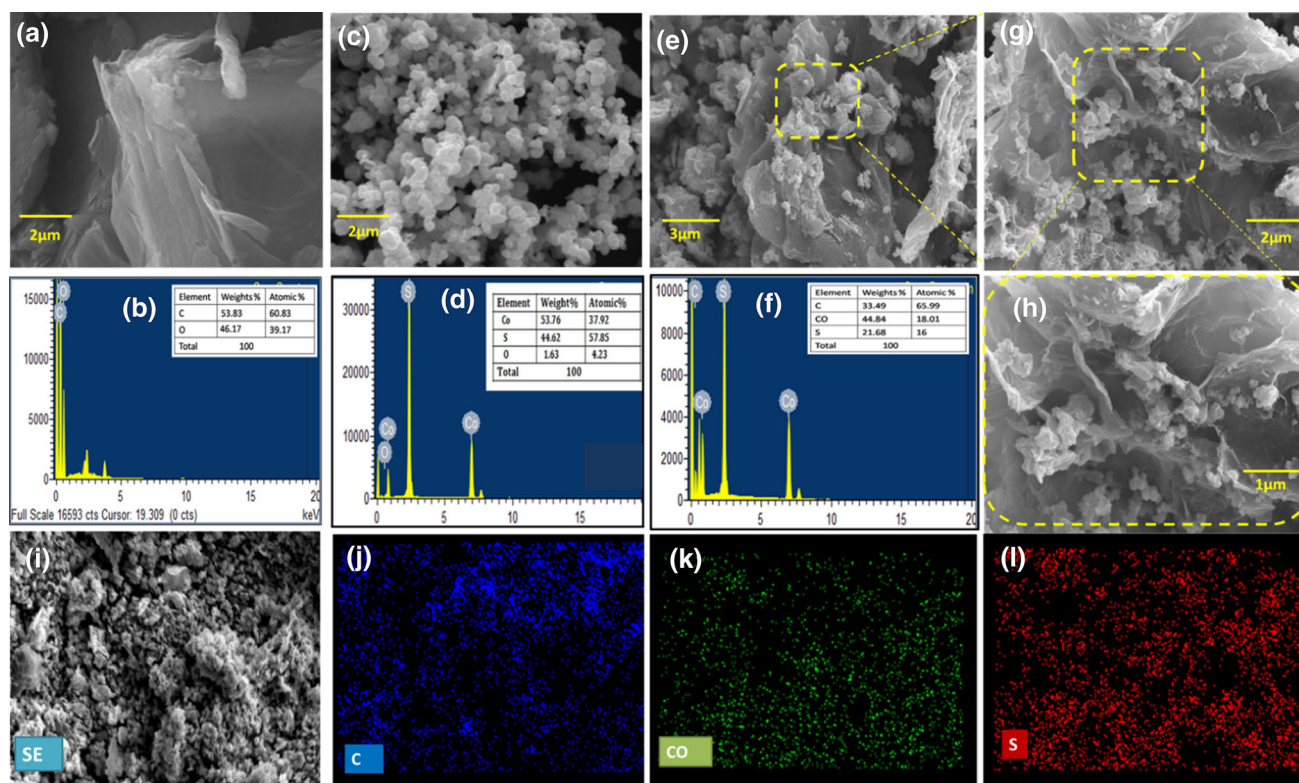
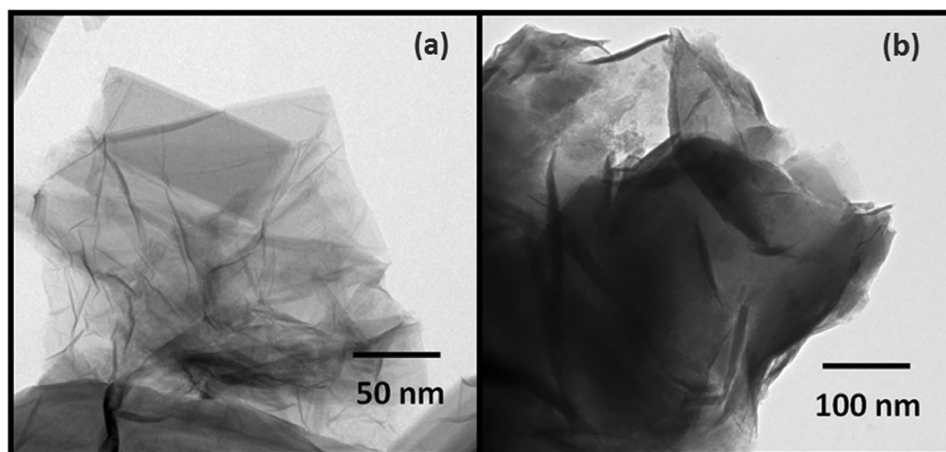


Fig. 4 SEM images and its corresponding EDAX spectrum of **a, b** Graphene oxide, **c, d** CoS NPs, **e–h** CoS/G nanocomposite. **i–l** EDS mapping images of Co, S, and C elements in the CoS/G nanocomposite

Fig. 5 TEM images of **a** Graphene oxide and **b** CoS/G nanocomposite



over the graphene sheet. From these results, the graphene acts as a buffer layer for decorating the CoS nanospheres. The carbon mapping indicates the layer of graphene where CoS nanoparticles are distributed throughout the area.

TEM measurements were performed to understand the clear morphology and size of the graphene oxide and CoS/G nanocomposite as shown in Fig. 5. The graphene oxide sheet shows a layered structure with several wrinkles on its surface, which is demonstrated in Fig. 5a. The TEM image in Fig. 5b reveals the homogenous distribution of spherical CoS nanoparticles on the surface of the graphene sheets, which were interconnected with each other, which is consistent with the scanning electron microscope results. The observed surface area is more advantageous for electrode and electrolyte interaction, which improves the stability and wettability as well as the electrochemical activity of the composite materials.

3.5 Surface area analysis

The specific surface area and pore size distribution of the prepared materials have been evaluated by Brunauer–Emmett–Teller (BET). Figure 6 demonstrates the N₂ adsorption–desorption isotherms of the prepared materials such as graphene oxide, pure CoS nanospheres, and CoS/G nanocomposite. Figure 6a displays the N₂ adsorption–desorption isotherms of the as-synthesized samples. A symbolic IV isotherm with an apparent hysteresis loop at various relative pressures (P/P_0) is present in both plots, which indicates the mesoporous structures. The pore size distribution of the obtained materials is shown in

Fig. 6b, where the CoS/G nanocomposite has a narrow distribution of pore size, primarily in the 2 to 3 nm range. On the other hand, CoS nanospheres show a broad size distribution compared to CoS/G nanocomposite. The values of $37.0 \text{ m}^2\text{g}^{-1}$ and $0.24 \text{ cm}^3\text{g}^{-1}$ are acquired from the BET surface area and the total CoS/G pore volume, respectively. The composite values are higher than those of CoS nanospheres ($14.3 \text{ m}^2\text{g}^{-1}$ and $0.10 \text{ cm}^3\text{g}^{-1}$). The CoS/G nanocomposite has a high surface area compared with pure CoS nanospheres. The presence of graphene oxide enhanced the surface area of the composite, which is expected to improve the specific capacitance of the supercapacitor appreciably.

3.6 Electrochemical measurements

The various techniques, including cyclic voltammetry, Galvanostatic charge–discharge, and electrochemical impedance measurements, were adopted to examine the electrochemical performance of the as-prepared materials. The experiment was conducted using a 3 M KOH three-electrode system under ambient conditions. Figure 7 demonstrates the CV curves of the prepared materials such as CoS nanospheres and CoS/G nanocomposite. The form of the CV curves indicates the presence of well-defined oxidation and reduction peaks, suggesting pseudocapacitance nature due to the Faradaic reaction that can be attributed to the CoS redox reactions in alkaline electrolytes [50]. In addition, the CoS/G nanocomposite depicted similar behaviors to the CoS nanospheres, which confirms the pseudocapacitive. In addition, the presence of graphene significantly enhances the integral area as well as the capacitive

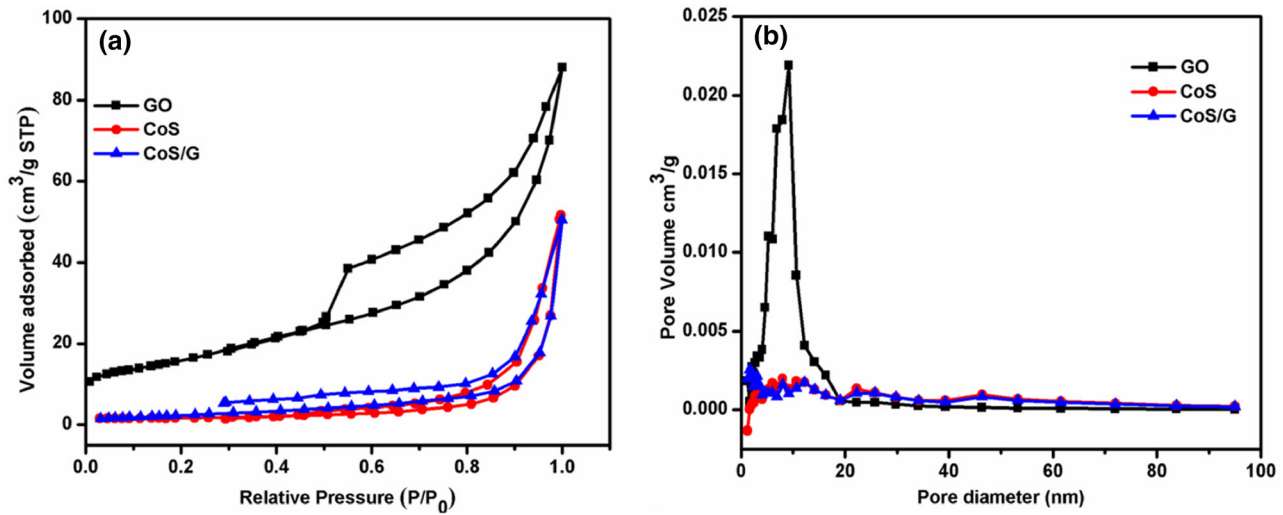
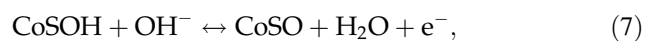
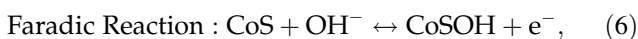
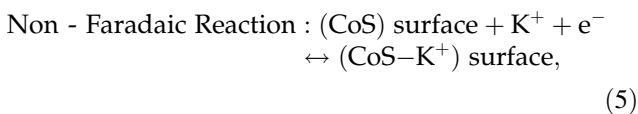


Fig. 6 **a** Nitrogen adsorption–desorption isotherm and **b** pore size distribution of GO, CoS nanospheres, and CoS/G nanocomposite

Table 1 The comparison of some other chalcogenide/graphene based electrode materials for supercapacitors applications

S. no.	Electrode materials	Electrolyte	Potential window (V)	Capacitance (F g ⁻¹)	Refs.
1	ZnS/graphene	2 M KOH	– 0.2 to 0.4	315	[53]
2	CdS/graphene	3 M KOH	0.0 to 1.0	248	[26]
3	SnS ₂ /graphene	3 M KOH	0.0 to 0.6	431.82	[54]
4	NiS/graphene	2 M KOH	0.0 to 0.5	1020	[29]
5	CoS/graphene	3 M KOH	0.0 to 0.6	739.83	This work

behavior of the material. Because the CoS nanospheres are uniform dispersion over the graphene sheets, it could be beneficial for electron transfer between the electrode and electrolyte [32]. At the lower scan rate, the electrolyte ions penetrate the interior surface of the electrode, which leads to higher capacitance. At a high scan rate, the electrolyte ions were blocked from the surface of the electrode due to insufficient time. The entire sweep rates possess the pair of redox peaks due to the reversible redox reaction of CoS (Co²⁺/Co³⁺) is converted into CoO or CoSOH. Besides, the adsorption/desorption of K⁺ ions on the surface of the electrode and the possibility of intercalation/deintercalation of K⁺ ions into or away from the surface of the CoS/G nanocomposite [33].



The integral areas of the CV curves have been increased gradually with increased scan rate and the redox peaks was shifted on both sides due to the internal diffusion resistance.

Figure 7c displays the specific capacitance of CoS nanospheres and CoS/G nanocomposite. This figure demonstrates that the increasing scan rates lead to a decrease in the specific capacitance for both materials, which is due to the fast sweep rates leading to the involvement of the outer porosity of the electrode material. Moreover, due to quick scan rates, deep/inner porosity of the electrode material is not accessible. The electrode was scanned superficially with a partial contribution, resulting in a low specific capacitance. The shape of CV curves does not change as the scanning rate rises from 10 to 200 mVs⁻¹, which is an excellent rate capability. Therefore, the CoS/G nanocomposite gives a larger current response, revealing a higher capacity for load storage and better capacitance performance [34]. The calculated specific capacitance of CoS/G (625.15 Fg⁻¹) is

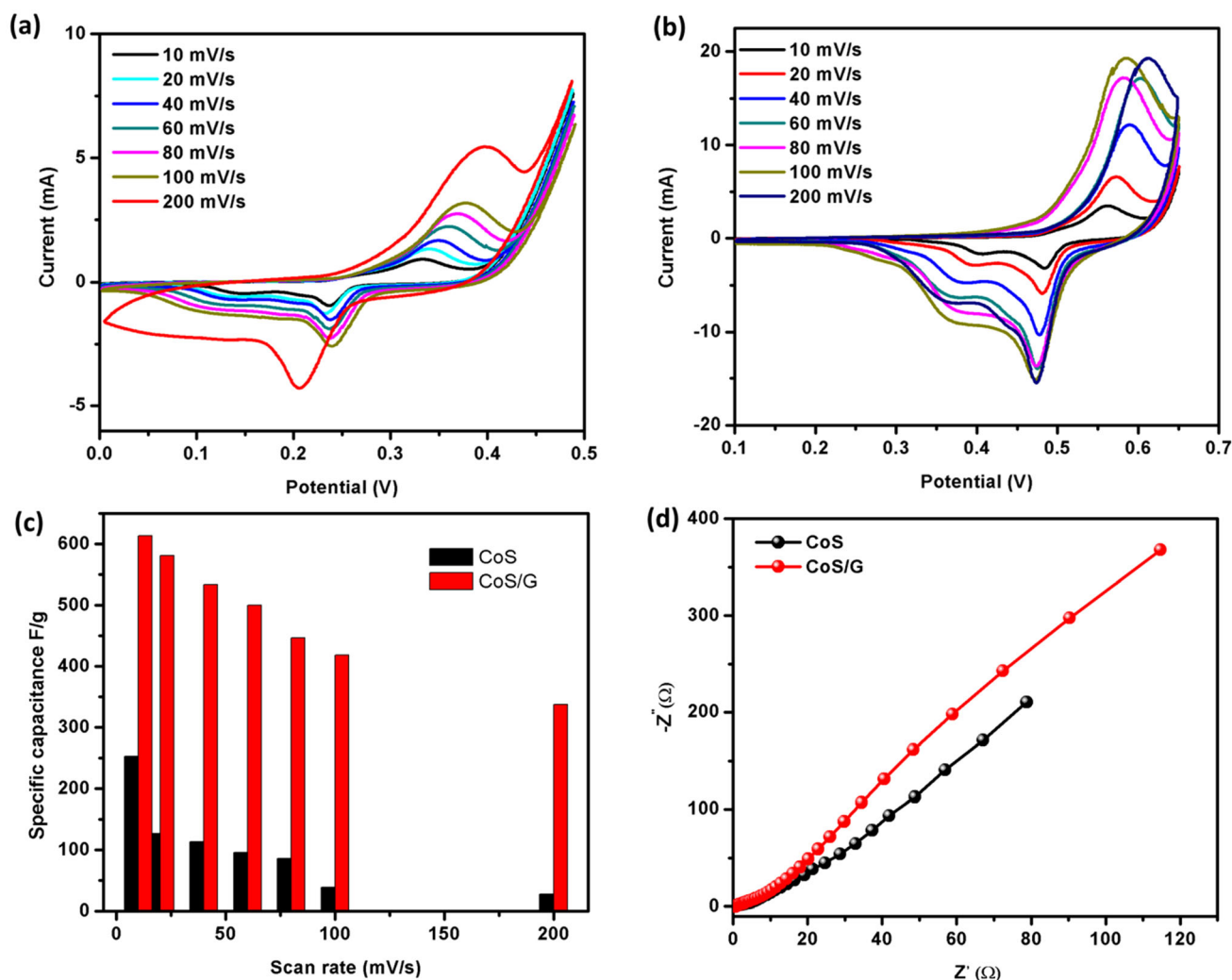


Fig. 7 Cyclic voltammety response of **a** pure CoS nanospheres and **b** CoS/G nanocomposite, **c** Specific capacitance of CoS nanospheres and CoS/G nanocomposite over various scan rates, **d** EIS profile of CoS nanospheres and CoS/G nanocomposite

much higher as compared to CoS (250.19 Fg^{-1}). The electrochemical performance of the CoS/graphene composite could be ascribed to the unique composite architecture of CoS nanospheres dispersed in the graphene sheet. Besides, graphene prevents the CoS nanospheres' agglomeration and also increases the surface area of the composite, which is beneficial for the electrolyte contact area of the composite electrode.

The electrical properties of the prepared materials have been elucidated by electrochemical impedance spectroscopy. Figure 7d demonstrates the Nyquist plot of CoS nanospheres and CoS/graphene nanocomposite electrodes. Both materials consist of one depressed semicircle in the high-frequency region and a straight line in the low-frequency

region. The width of the semicircle describes the interfacial load-transfer resistance (R_{ct}) associated with the electrode charge-transfer kinetics in the electrolyte solution. The CoS/G nanocomposite has a slightly smaller R_{ct} than the CoS nanospheres. The smaller R_{ct} value is beneficial for a higher specific capacity [51]. The high slope of the CoS/G nanocomposite suggests faster ion transfer rates between the electrolyte and the electrode. In comparison, CoS nanoparticles have a smaller vertical line than composite materials, this indicates the CoS/G nanocomposite more suitable pseudocapacitors model [52]. The above electrochemical impedance spectroscopy tests cogently prove that CoS/G imparts dominance in ion diffusion and electrochemical kinetics compared to CoS nanospheres,

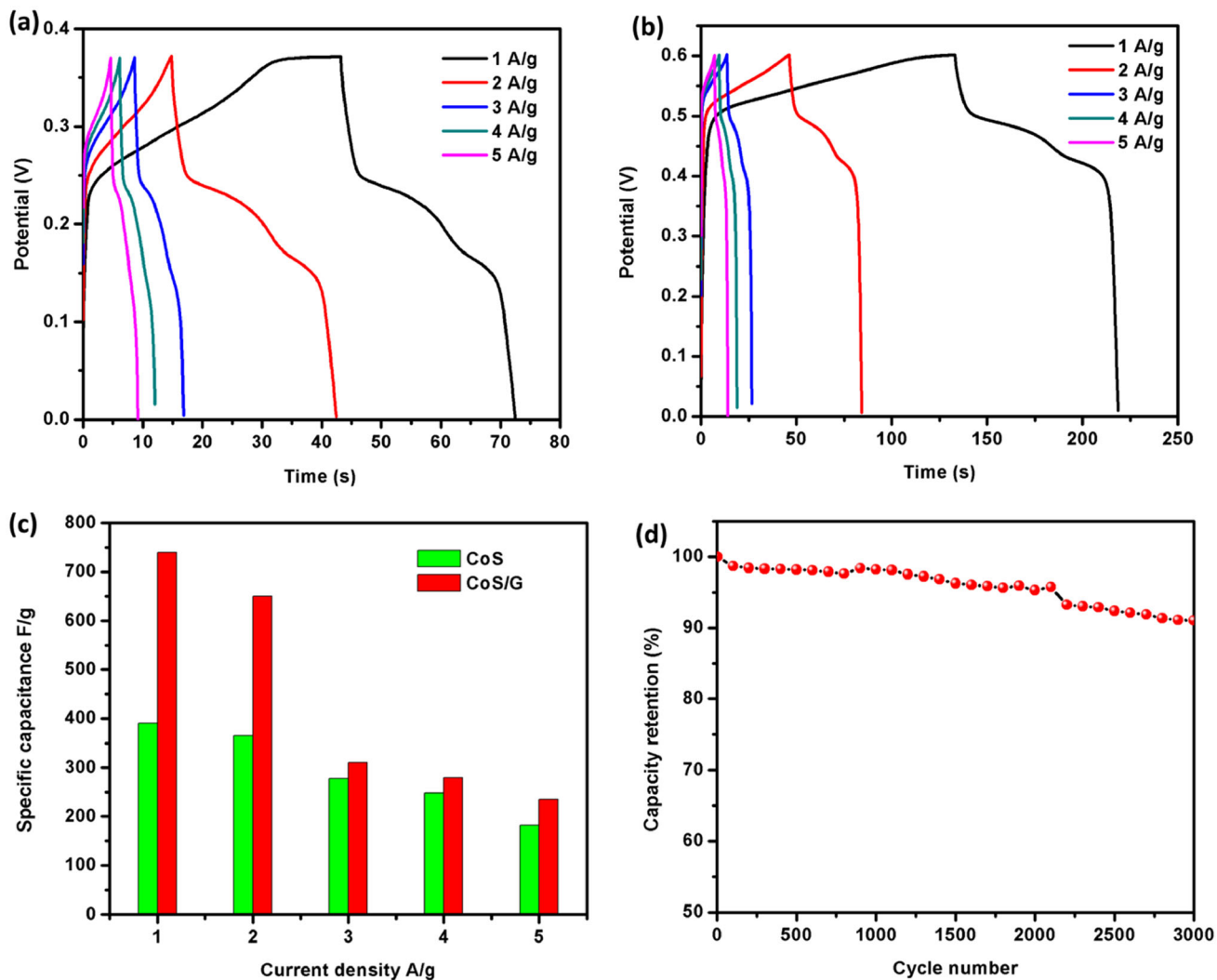


Fig. 8 Galvanostatic charge/discharge behavior of **a** CoS nanospheres, **b** CoS/G nanocomposite, **c** Specific capacitance of CoS nanospheres and CoS/G nanocomposite at various current densities **d** Cyclic stability of CoS nanospheres and CoS/G nanocomposite

thereby demonstrating enhanced efficiency for supercapacitors. It is known that the long-term cyclic stability of a supercapacitor is also an important parameter when applied in real-time practical applications.

The Galvanostatic charge–discharge curves of the prepared materials such as CoS and CoS/G nanocomposite at various current densities are depicted in Fig. 8. The CoS nanospheres curve shows the plateau and a non-linear relationship of potential time, furthermore the Faradic reaction between electrode and the electrolytes, which is confirming the pseudocapacitive nature. Figure 8b demonstrates the charge–discharge curve of CoS/G nanocomposite at different densities of 1 to 5 Ag⁻¹ and it is evident that the triangles in charge–discharge plots are not

symmetrical enough as evidenced by the specific property of CoS during the discharge process. The specific capacitance of the materials calculated from Eq. (2), the obtained specific capacitances of both electrode values are given. Interestingly, the current density values increased with decreasing the capacitance slowly it demonstrating the inverse relationship between the specific capacitance and current densities. This is because of time constraints for OH⁻ to diffuse into the electrode due to high current densities, while at a low current density OH⁻ ions have sufficient time to diffuse into the electrode material which results in higher specific capacitance values. The CoS NPs decorated on graphene sheets have shown higher efficiency due to their conducting nature and low charge-transfer resistance.

Furthermore, CoS NPs helped the graphene sheets by preventing them from wrinkles which facilitates the flow of electrons. The charge–discharge time of pure CoS electrodes is small, whereas it has been considerably improved in the nanocomposite. This composite matrix indicates the high charge capacity due to the presence of graphene. It could act as a buffer layer in the composite which enhances the electron bath way.

The electrochemical cyclic stability of the CoS/G nanocomposite for 3000 cycles at a current density of 5 Ag^{-1} . After being cycled for 3000 cycles, the CoS/G nanocomposite reveals 92.68% outstanding performance and demonstrating in Fig. 8d. This may be Incorporating graphene sheets in composite is expected to improve cyclic stability, mainly due to their high mechanical strengths enhanced the cyclic performance during the process. CoS/G nanocomposite is capable electrode for enhancing the electrochemical performance of supercapacitor device. Some recent supercapacitor publications are summarized in Table 1. CoS/G nanocomposite possesses a higher specific capacitance than other compared materials.

4 Conclusion

In conclusion, the CoS nanospheres decorated with graphene nanocomposite have been synthesized by a facile hydrothermal method. The as-prepared materials were analyzed by various techniques to determine their structural and optical properties. The fabricated electrodes were investigated in a three-electrode configuration. The CoS/G nanocomposite demonstrated high specific capacitance 739.83 Fg^{-1} compared to the pure CoS nanospheres 390 Fg^{-1} and outstanding cyclic stability after 3000 cycles of retention withstands up to 92.68%. These enhances electrochemical properties of the CoS/G nanocomposite make it a noticeable candidate for high-performance supercapacitor devices.

Author contributions

RB: Preparation of samples, Collection of data, and Manuscript drafting, AD: Investigation and analysis of data, Writing-review & editing.

Funding

The authors have not disclosed any funding.

Data availability

Authors can confirm that all relevant data are included in the article.

Declarations

Conflict of interest The authors declare that they have no known competing financial interests or personal relationships that could have appeared to influence the work reported in this paper.

References

1. P. Simon, Y. Gogotsi, Materials for electrochemical capacitors. *Nat. Mater.* **7**, 845–854 (2008)
2. Y. Xiaowei, Z. Junwu, Q. Ling, L. Dan, Bioinspired effective prevention of restacking in multilayered graphene films: towards the next generation of high-performance supercapacitors. *Adv. Mater.* **23**, 2833–2838 (2011). <https://doi.org/10.1002/adma.201100261>
3. Z. Haitao, Z. Xiong, Z. Dacheng, S. Xianzhong, He. Lin, W. Changhui, M. Yanwei, One-step electrophoretic deposition of reduced graphene oxide and $\text{Ni}(\text{OH})_2$ composite films for controlled syntheses supercapacitor electrodes. *J. Phys. Chem. B* **117**, 1616–1627 (2013). <https://doi.org/10.1021/jp305198j>
4. K. Seevakan, A. Manikandan, P. Devendran, Y. Slimani, A. Baykal, T. Alagesan, Structural, magnetic and electrochemical characterizations of $\text{Bi}_2\text{Mo}_2\text{O}_9$ nanoparticle for supercapacitor application. *J. Magn. Magn Mater* **486**(15), 165254 (2019)
5. K. Seevakan, A. Manikandan, P. Devendran, Y. Slimani, A. Baykal, T. Alagesan, Structural, morphological and magneto-optical properties of CuMoO_4 electrochemical nanocatalyst as supercapacitor electrode. *Ceram. Int.* **44**(16), 20075–20083 (2018)
6. O.G. Gnonhoue, A. Velazquez-Salazar, É. David, I. Preda, Review of technologies and materials used in high-voltage film capacitors. *Polymers* **13**(5), 766 (2021). <https://doi.org/10.3390/polym13050766>
7. A. Abdelkareem, M. Ali, E. Khaled, W. Tabbi, K. Mohammed, S.E. Taha, A. Olabi, Environmental aspects of fuel cells: a review. *Sci. Total Environ.* **752**, 141803 (2020). <https://doi.org/10.1016/j.scitotenv.2020.141803>

8. Z. Luojiang, W. Haitao, Z. Xiaoming, T. Yongbing, A review of emerging dual-ion batteries: fundamentals and recent advances. *Adv. Func. Mater.* **31**, 20 (2021). <https://doi.org/10.1002/adfm.202010958>
9. J. Xie, Y.C. Lu, A retrospective on lithium-ion batteries. *Nat. Commun.* **11**, 2499 (2020). <https://doi.org/10.1038/s41467-020-16259-9>
10. Z. Meng, L. Bo-Quan, Z. Xue-Qiang, H. Jia-Qi, Z. Qiang, A perspective toward practical lithium-sulfur batteries *ACS cent. Sci.* **6**(7), 1095–1104 (2020)
11. K. Binoy, S. Saikia, B. Maria, B. Mousumi, T. Joyshil, P. Mayank, B. Dhurbajyoti, A brief review on supercapacitor energy storage devices and utilization of natural carbon resources as their electrode materials. *Fuel* **282**, 118796 (2020). <https://doi.org/10.1016/j.fuel.2020.118796>
12. R. Chen, Y. Miao, R.P. Sahu, K.P. Ishwar, Z. Igor, The development of pseudocapacitor electrodes and devices with high active mass loading. *Adv. Energy Mater.* (2020). <http://doi.org/10.1002/aenm.201903848>
13. L.L. Zhang, R. Zhou, X.S. Zhao, Graphene-based materials as supercapacitor electrodes. *J. Mater. Chem.* **20**, 5983–5992 (2010). <https://doi.org/10.1039/C000417K>
14. R. Dubey, V. Guruviah, Review of carbon-based electrode materials for supercapacitor energy storage. *Ionics* **25**(4), 1419–1445 (2019). <https://doi.org/10.1007/s11581-019-02874-0>
15. X. Zhang, H. Zhang, Z. Lin, M. Yu, X. Lu, Y. Tong, Recent advances and challenges of stretchable supercapacitors based on carbon materials. *Sci. China Mater.* **59**(6), 475–494 (2016). <https://doi.org/10.1007/s40843-016-5061-1>
16. I.K. Durga, S.S. Rao, M. Jagadeesh, A.E. Reddy, T. Anitha, H.J. Kim, Synthesis of nanostructured metal sulfides via a hydrothermal method and their use as an electrode material for supercapacitors. *New J. Chem.* **42**, 19183–19192 (2018)
17. R. Chen, Y. Miao, R.P. Sahu, K.P. Ishwar, I. Zhitomirsky, The development of pseudocapacitor electrodes and devices with high active mass loading. *Adv. Energy Mater.* (2020). <http://doi.org/10.1002/aenm.201903848>
18. V. Augustyn, P. Simon, B. Dunn, Pseudocapacitive oxide materials for high-rate electrochemical energy storage. *Energy Environ. Sci.* **7**(5), 1597–1614 (2014). <https://doi.org/10.1039/C3EE44164D>
19. S. Khamlich, Z. Abdullaeva, J.V. Kennedy, M. Maaza, High performance symmetric supercapacitor based on zinc hydroxychloride nanosheets and 3D graphene-nickel foam composite. *Appl. Surf. Sci.* **405**(31), 329–336 (2017)
20. J. Ge, B. Wang, J. Wang, Q. Zhang, B. Lu, Nature of FeSe₂/N-C anode for high performance potassium ion hybrid capacitor. *Adv. Energy Mater.* **10**(4), 1903277 (2020)
21. Y. Zhu, S. Murali, W. Cai, X. Li, J.W. Suk, J.R. Potts, R.S. Ruoff, Graphene and graphene oxide: synthesis, properties, and applications. *Adv. Mater.* **22**, 3906–3924 (2010). <https://doi.org/10.1002/adma.201001068>
22. K. Suenne, Z. Si, H. Yike, A. Muge, J. Yves, C.B. Chabal, H. de Walt, B. Angelo, R. Elisa, Room-temperature metastability of multilayer graphene oxide films. *Nat. Mater.* **11**, 544–549 (2012). <https://doi.org/10.1038/nmat3316>
23. W. Sun, G. Gao, Y. Du, K. Zhang, G. Wu, A facile strategy for fabricating hierarchical nanocomposites of V₂O₅ nanowire arrays on a three-dimensional N-doped graphene aerogel with a synergistic effect for supercapacitors. *J. Mater. Chem. A* **6**, 9938–9947 (2018)
24. K. Gopalakrishnan, S. Sultan, A. Govindaraj, C.N.R. Rao, Supercapacitors based on composites of PANI with nanosheets of nitrogen doped RGO, BC_{1.5}N, MoS₂ and WS₂. *Nano Energy* **12**, 52–58 (2015)
25. B. Xie, Y. Chen, Yu. Mengying, Tu. Sun, Lu. Luhua, T. Xie, Y. Zhang, Wu. Yucheng, Hydrothermal synthesis of layered molybdenum sulfide/N-doped graphene hybrid with enhanced supercapacitor performance. *Carbon* **99**, 35–42 (2016). <http://doi.org/10.1016/j.carbon.2015.11.077>
26. R. Balu, A. Dakshanamoorthy, A simple hydrothermal synthesis of cadmium sulfide wrapped on graphene nanocomposite for supercapacitor applications. *J. Nanosci. Nanotechnol.* **21**(12), 5835–5845 (2021). <https://doi.org/10.1166/jnn.2021.19503>
27. R. Balu, A. Dakshanamoorthy, Synthesis of wool ball-like copper sulfide nanospheres embedded graphene nanocomposite as electrode for high performance symmetric supercapacitor device. *Int. J. Energy Res.* **24**, 1–15 (2021)
28. R. Balu, A. Dakshanamoorthy, One-pot preparation of tin sulfide decorated graphene nanocomposite for high performance supercapacitor applications. *Inorg. Chem. Commun.* **136**, 109148 (2022)
29. C.A. Pandey, S. Ravuri, R. Ramachandran, R. Santhosh, S. Ghosh, S.R. Sitaraman, A.N. Grace, Grace synthesis of NiS–graphene nanocomposites and its electrochemical performance for supercapacitors. *Int. J. Nanosci.* **17**, 1760021 (2018). <https://doi.org/10.1142/S0219581X17600213>
30. R. Ramachandran, M. Saranya, P. Kollu, B.P. Raghupathy, S.K. Jeong, A.N. Grace, Solvothermal synthesis of Zinc sulfide decorated Graphene (ZnS/G) nanocomposites for novel supercapacitor electrodes. *Electrochim. Acta* **178**(1), 647–657 (2015)
31. M. Mao, L. Mei, L. Wu, Q. Li, M. Zhang, Facile synthesis of cobalt sulfide/carbon nanotube shell/core composites for high performance supercapacitors. *RSC Adv.* **4**, 12050–12056 (2014). <https://doi.org/10.1039/C4RA00485J>

32. F. Tao, Y.Q. Zhao, G.Q. Zhang, H.L. Li, Electrochemical characterization on cobalt sulfide for electrochemical supercapacitors. *Electrochem. Commun.* **9**, 1282–1287 (2007). <https://doi.org/10.1016/j.elecom.2006.11.022>
33. K.J. Huang, J.Z. Zhang, G. Shi, Y.M. Shi, One-step hydrothermal synthesis of two-dimensional cobalt sulfide for high-performance supercapacitors. *Mater. Lett.* **131**, 45–48 (2014). <https://doi.org/10.1016/j.matlet.2014.05.148>
34. Z. Yang, C.Y. Chen, H.T. Chang, Supercapacitors incorporating hollow cobalt sulfide hexagonal nanosheets. *J. Power Sources* **196**, 7874–7877 (2011). <https://doi.org/10.1016/j.jpowsour.2011.03.072>
35. K.J. Huang, J.Z. Zhang, G.W. Shi, Y.M. Liu, One-step hydrothermal synthesis of two-dimensional cobalt sulfide for high-performance supercapacitors. *Mater. Lett.* **131**, 45–48 (2014). <https://doi.org/10.1016/j.matlet.2014.05.148>
36. M.M. Shahid, A. Pandikumar, A.M. Golsheikh, N.M. Huang, H.N. Lim, Enhanced electrocatalytic performance of cobalt oxide nanocubes incorporating reduced graphene oxide as a modified platinum electrode for methanol oxidation. *RSC Adv.* **4**, 62793–62801 (2014). <https://doi.org/10.1039/C4RA08952A>
37. S.J. Peng, L.L. Li, X.P. Han, W.P. Sun, M. Srinivasan, F.Y. Cheng, Q.Y. Yan, J. Chen, S. Ramakrishna, Cobalt sulfide nanosheet/graphene/carbon nanotube nanocomposites as flexible electrodes for hydrogen evolution. *Angew. Chem. Int. Ed.* **53**, 12594–12599 (2014). <https://doi.org/10.1002/anie.201408876>
38. W.S. Hummers Jr., R.E. Offeman, Preparation of graphitic oxide. *J. Am. Chem. Soc.* **80**, 1339–1339 (1958)
39. E. Sathiyaraj, S. Thirumaran, Structural, morphological and optical properties of iron sulfide, cobalt sulfide, copper sulfide, zinc sulfide and copper-iron sulfide nanoparticles synthesized from single source precursors. *Chem. Phys. Lett.* (2019). <https://doi.org/10.1016/j.cplett.2019.136972>
40. F. Tuinstra, J.L. Koenig, Raman spectrum of graphite. *J. Chem. Phys.* **53**, 1126–1130 (1970). <https://doi.org/10.1063/1.1674108>
41. C.J. Fu, G.G. Zhao, H.J. Zhang, S. Li, A facile route to controllable synthesis of Fe₃O₄/graphene composites and their application in lithium-ion batteries. *Int. J. Electrochem. Sci.* **9**, 46–60 (2014)
42. S. Stankovich, D.A. Dikin, R.D. Piner, K.A. Kohlhaas, A. Kleinhammes, Y.Y. Jia, Y. Wu, S.T. Nguyen, R.S. Ruoff, Synthesis of graphene-based nanosheets via chemical reduction of exfoliated graphite oxide. *Carbon* **45**, 1558–1565 (2007). <https://doi.org/10.1016/j.carbon.2007.02.034>
43. C. Xu, Y. Jing, J.R. He, K.R. Zhou, Y.F. Chen, Q. Li, J. Lin, W.L. Zhang, Self-assembled interwoven CoS₂/CNTs/graphene architecture as anode for high-performance lithium ion batteries. *J. Alloys Compd.* **708**, 1178–1183 (2017). <https://doi.org/10.1016/j.jallcom.2017.03.099>
44. R. Ramachandran, S. Felix, M. Saranya, C. Santhosh, V. Velmurugan, B.P. Ragupathy, S.K. Jeong, A.N. Grace, Synthesis of cobalt sulfide-graphene (CoS/G) nanocomposites for supercapacitor applications. *IEEE Trans. Nanotechnol.* **12**, 985–990 (2013). <https://doi.org/10.1109/TNANO.2013.2278287>
45. V. Chabot, D. Higgins, A. Yu, X. Xiao, Z. Chena, J. Zhang, A review of graphene and graphene oxide sponge: Material synthesis and applications to energy and the environment. *Energy Environ. Sci.* **7**, 1564–1596 (2014). <https://doi.org/10.1039/C3EE43385D>
46. M. Jianfei, S. Qian, W. Yaqiong, Y. Hongyan, X. Dan, M.M.F. Choi, Facile fabrication of porous CuS nanotubes using well-aligned [Cu(tu)]Cl·1/2H₂O nanowire precursors as self-sacrificial templates. *Cryst. Growth Des.* **9**, 2546–2548 (2009). <https://doi.org/10.1021/cg8006052.7>
47. L. Guojun, C. Lili, W. Yanying, L. Ying, P. Tao, X. He, A novel cobalt tetranitrophthalocyanine/graphene composite assembled by an in situ solvothermal synthesis method as a highly efficient electrocatalyst for the oxygen reduction reaction in alkaline medium. *Phys. Chem. Chem. Phys.* **31**, 13093–13100 (2013). <https://doi.org/10.1039/C3CP51577J>
48. T.F. Emiru, D.W. Ayele, Controlled synthesis, characterization and reduction of graphene oxide: a convenient method for large scale production. *Egypt. J. Basic Appl. Sci.* **4**(1), 74–79 (2017)
49. Q. Wang, L. Jiao, H. Du, Y. Si, Y. Wang, H. Yuan, Co₃S₄ hollow nanospheres grown on graphene as advanced electrode materials for supercapacitors. *J. Mater. Chem.* **22**, 21387–21391 (2012). <https://doi.org/10.1039/C2JM34714H>
50. J. Zhu, W. Zhou, Y. Zhou, X. Cheng, J. Yang, Cobalt Sulfide/reduced graphene oxide nanocomposite with enhanced performance for supercapacitors. *J. Electron. Mater.* **48**, 3 (2019). <https://doi.org/10.1007/s11664-018-06910-z>
51. S. Muhammad Mehmood, R. Perumal, P. Alagarsamy, L. Hong Ngee, N. Yun Hau, H. Nay Ming, An electrochemical sensing platform based on a reduced graphene oxide-cobalt oxide nanocube@ platinum nanocomposite for nitric oxide detection. *J. Mater. Chem. A* **3**, 14458–14468 (2015). <https://doi.org/10.1039/C5TA02608C>
52. K. Subramani, N. Sudhan, R. Divya, M. Sathish, All-solid-state asymmetric supercapacitors based on cobalt hexacyanoferrate-derived CoS and activated carbon. *RSC Adv.* **7**, 6648–6659 (2017). <https://doi.org/10.1039/C6RA27331A>
53. R. Balu, S. Sagadevan, A. Dakshnamoorthy, A cost effective, facile hydrothermal approach of zinc sulfide decorated on graphene nanocomposite for supercapacitor applications.

- J. Nanosci. Nanotechnol. **19**, 6987–6994 (2019). <https://doi.org/10.1166/jnn.2019.16670>
54. H. Chauhan, M.K. Singh, P. Kumar, S.A. Hashmi, S. Deka, Development of SnS₂/rGO nanosheet composite for cost-effective aqueous hybrid supercapacitors. Nanotechnology **28**(2), 025401 (2016). <https://doi.org/10.1088/1361-6528/28/2/025401>

Publisher's Note Springer Nature remains neutral with regard to jurisdictional claims in published maps and institutional affiliations.